

# Geophysical Research Letters

## RESEARCH LETTER

10.1029/2019GL085910

### Key Points:

- Cross strata are dominantly built during flood recession due to enhanced localized sedimentation rates, relative to bedform migration rates
- The ratio of time scales of flood variability and bedform adjustment is reflected in the coefficient of variation of preserved cross sets
- Global bedform and flood discharge data sets suggest that bedform disequilibrium dynamics are the norm in modern rivers and ancient deposits

### Supporting Information:

- Supporting Information S1
- Table S1

### Correspondence to:

K. C. P. Leary,  
learykcp@ucsb.edu

### Citation:

Leary, K. C. P., & Ganti, V. (2020). Preserved fluvial cross strata record bedform disequilibrium dynamics. *Geophysical Research Letters*, 47, e2019GL085910. <https://doi.org/10.1029/2019GL085910>

Received 18 OCT 2019

Accepted 9 DEC 2019

Accepted article online 13 DEC 2019

## Preserved Fluvial Cross Strata Record Bedform Disequilibrium Dynamics

Kate C. P. Leary<sup>1</sup>  and Vamsi Ganti<sup>1,2</sup> 

<sup>1</sup>Department of Geography, University of California, Santa Barbara, CA, USA, <sup>2</sup>Department of Earth Science, University of California, Santa Barbara, CA, USA

**Abstract** Fluvial cross strata are an archive of ancient river morphodynamics. Controls on their preservation are well documented for bedforms equilibrated with prevailing flows; however, variability in water and sediment discharge results in bedforms that are routinely out of phase with flow conditions—termed bedform disequilibrium. Using theory and experiments of dune evolution in steady and unsteady flows, we show that preservation of cross strata is greater during unsteady flows—particularly during flood recession—when bedform disequilibrium is prevalent. The enhanced preservation of disequilibrium dynamics is associated with a high bedform preservation ratio, which results from localized increase in sedimentation rates relative to bedform migration rates due to the hierarchical bedform organization during flood recession. We find that the coefficient of variation of cross sets reflects the ratio of the time scales of formative-flood variability and bedform adjustment. We parameterize bedform disequilibrium for rivers globally and suggest that flood variability is a key control on cross set preservation.

**Plain Language Summary** Undulating topographic features such as ripples, dunes, and bars—called bedforms—abound on riverbeds worldwide. Bedform migration results in cross-stratified rock units, which are ubiquitous sedimentary features on Earth and Mars. Cross-stratified sandstones provide a window into the hydrological cycle as well as the mass fluxes that rivers carried from mountains to the sea in ancient environments. Consequently, controls on the preservation of cross strata have been studied for over a century, but the majority of this work focused on bedform evolution in steady flows. Floods, however, cause water and sediment discharge to vary continuously in rivers, which significantly affect bedform evolution. Despite this recognition, we currently lack a quantitative understanding of the influence of flow variability on fluvial cross strata. We addressed this knowledge gap using theory and laboratory experiments. We find that the preservation of cross strata preferentially occurs during flood recession, even if this duration is a small fraction of total time. We uncovered statistical metrics that can help decipher the nature of flood discharge variability from the geometry of cross-stratified rock units, with implications for quantifying river dune dynamics and flood variability on ancient Earth and Mars.

## 1. Introduction

Ripples, dunes, and bars—all called bedforms—abound on alluvial riverbeds across a range of grain sizes and channel patterns (Best, 2005; Carling, 1999; Ganti et al., 2014; Hajek & Straub, 2017; Ohata et al., 2017; Southard, 1991). Bedform migration results in cross stratification, which is a key building block of alluvium on planetary bodies (e.g., Allen, 1982a; Best & Fielding, 2019; Edgar et al., 2018; Rubin & Hunter, 1982). Bedform geometry and kinematics scale with flow, sediment transport, and bed composition (Baas et al., 2016; Bradley & Venditti, 2017, 2019a, 2019b; Parsons et al., 2016; Southard, 1991; Van Rijn, 1984; Yalin, 1964), and cross stratification archives ancient river morphodynamics (Jerolmack & Mohrig, 2005; Leclair & Bridge, 2001; Mahon & McElroy, 2018; Paola & Borgman, 1991; Reesink et al., 2015). Empirical relations between bedform geometry and their formative conditions inform the estimation of paleoflow depths (Bradley & Venditti, 2017; Leclair & Bridge, 2001), bedload fluxes (Mahon & McElroy, 2018), paleofluvial gradients (Ganti, Whittaker, et al., 2019), paleoflow velocity (Bhattacharya & Tye, 2004; Ohata et al., 2017), and duration of fluvial activity on Mars (Edgar et al., 2018), for example. Thus, understanding the controls on cross strata preservation is essential for quantifying paleohydrology and sediment discharge in ancient sedimentary environments.

The controls on the geometry of fluvial cross strata have been researched for over a century (e.g., Allen, 1973a; Ganti et al., 2013; Gilbert, 1899; Jerolmack & Mohrig, 2005; Leclair & Bridge, 2001; Paola & Borgman, 1991; Reesink et al., 2015; Rubin & Hunter, 1982; Sorby, 1859). Theory and experiments have led to the development of scaling relations between the preserved set thickness ( $d_{st}$ )—thickness of the deposits bounded by successive erosional boundaries—and the formative bedform geometry, parameterized by bedform height ( $h_d$ ) and length ( $\lambda$ ), at statistical steady state during constant flows (e.g., Jerolmack & Mohrig, 2005; Leclair, 2002). Paola and Borgman (1991) showed that the variability in bedform trough scour depths controls the set thickness distribution under no net aggradation conditions, and the coefficient of variation (ratio of standard deviation to mean) of the preserved sets is constant ( $CV(d_{st}) = 0.88$ ). The bedform preservation ratio, defined as the mean set thickness ( $s_m$ ) normalized by the average formative bedform height ( $h_m$ ), was shown to be relatively constant (~0.3) for small bedform climb angles ( $<10^{-2}$ ) across a range of steady flow conditions (Jerolmack & Mohrig, 2005; Leclair & Bridge, 2001). This variability-dominated preservation model ( $s_m/h_m \approx 0.3$ ;  $CV(d_{st}) \approx 0.88$ ) (cf. Reesink et al., 2015) was validated using experiments and numerical models (Ganti et al., 2013; Jerolmack & Mohrig, 2005; Leclair, 2002). In addition to variability of trough depths, bedform kinematics such as the migration rate and climb angle also influence the set thickness distribution and stratal geometries (Bridge & Best, 1997; Ganti et al., 2013; Jerolmack & Mohrig, 2005; Reesink et al., 2015).

While the aforementioned advances were instrumental in illuminating how bedform evolution is recorded in cross strata, they primarily addressed controls on cross stratification at steady state. Field observations, however, indicate that bedforms may seldom be equilibrated with prevailing flows—a phenomenon termed “bedform disequilibrium” (Myrow et al., 2018)—because sediment and water discharge vary naturally in rivers. Whereas hydrodynamic changes occur instantaneously, changes in bedform geometry require mass redistribution that occurs on longer time scales, leading to a phase lag between the prevailing flow conditions and bedform evolution (e.g., Figure 1a; Allen, 1973b; Myrow et al., 2018). Bedform adjustment requires the displacement of the sediment volume in a bedform, and the bedform “turnover time scale” ( $T_t$ ) is given by (e.g., Allen, 1973b; Martin & Jerolmack, 2013; Myrow et al., 2018)

$$T_t = \lambda h_d \beta / q_s \quad (1)$$

where  $q_s$  is the unit sediment flux and  $\beta \sim 0.55$  is the bedform shape factor. Myrow et al. (2018) defined a dimensionless bedform disequilibrium number ( $T^*$ ) as

$$T^* = \frac{T_f}{T_t} \quad (2)$$

where  $T_f$  is the duration of the prevailing flow. For  $T^* > 1$ , flow duration is sufficiently long for the bedforms to equilibrate; however, for  $T^* < 1$ , flow variation outpaces bedform adjustment, causing bedform disequilibrium.

The  $T^*$  framework also encapsulates the mechanistic differences between bedform growth and decay (Myrow et al., 2018). Experimental and field observations indicate that bedform growth occurs rapidly by bedform merger owing to their smaller dimensions (low  $T_t$ ; equation (1)), such that bedform size and water discharge evolve in phase (Figure 1a; Martin & Jerolmack, 2013; Reesink et al., 2018). In contrast, peak-flood-equilibrated bedform evolution lags behind waning flow because bedform adjustment to a reduction in water and sediment discharge occurs via cannibalization of relict bedforms by prevailing smaller, superimposed bedforms (Figure 1a). The cannibalization process has a large  $T_t$  (in equation (1),  $q_s$  decreases and bedform dimensions are large), leading to the out-of-phase evolution of bedforms and water discharge (Figure 1a; Myrow et al., 2018; Reesink et al., 2018). These differences between bedform growth and decay causes bedform hysteresis (e.g., Allen, 1974, 1976; Frings & Kleinhans, 2008; Julien et al., 2002; Ten Brinke et al., 1999; Wilbers & Ten Brinke, 2003), a commonly observed phenomenon wherein bedforms have a different size for the same water discharge on the rising and falling limb of a hydrograph.

While field observations suggest that bedform disequilibrium may be prevalent, we lack a quantitative understanding of how disequilibrium dynamics contribute to cross-stratal preservation. Here, using theory and experiments, we investigate the influence of flood hydrographs on preserved cross strata. We begin with

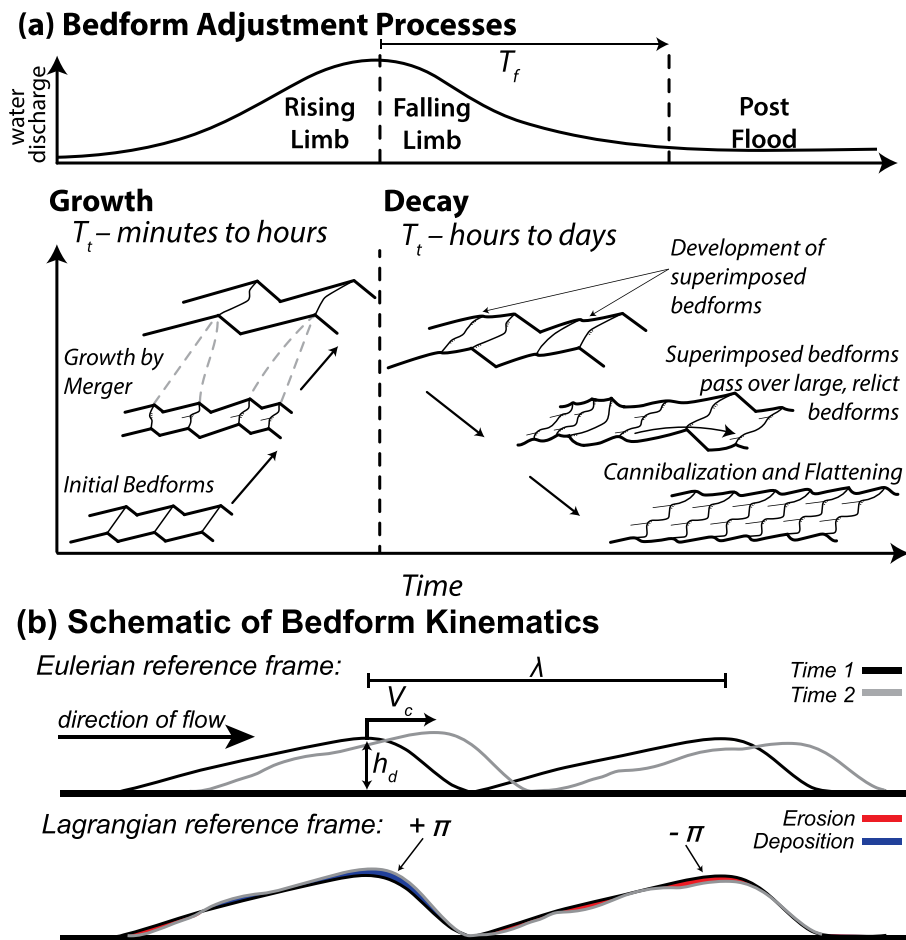


**Figure 1.** Schematics of (a) bedform adjustment through a flood hydrograph highlighting the bedform growth and decay processes (after Myrow et al., 2018), and (b) kinematic evolution of bedforms in Eulerian and Lagrangian frameworks, where the gray profile is at a later time than the black profile.

a summary of theoretical frameworks for the kinematic evolution of bedforms and controls on cross-stratal preservation.

## 2. Theory

McElroy and Mohrig (2009) proposed a unifying framework for kinematic evolution of transverse, unidirectional bedforms, given by

$$\frac{\partial \eta(x, t)}{\partial t} + V_c(t) \frac{\partial \eta(x, t)}{\partial x} = \Pi(x, t) \quad (3)$$

where  $V_c$  is the characteristic bedform migration rate,  $\Pi$  is the deformation rate,  $\eta$  is the bed elevation, and  $t$  and  $x$  are the time and streamwise distance, respectively (Figure 1b). The deformation rate quantifies bed elevation changes in a Lagrangian framework (McElroy & Mohrig, 2009), and it can be decomposed into a net aggradation rate ( $r$ ) and stochastic variations in local sedimentation rates ( $\pi$ ), that is,  $\Pi(x, t) = r + \pi(x, t)$  (Ganti et al., 2013). When  $\pi(x, t) = 0$ , bedforms are translationally invariant, whereas  $\pi(x, t) > 0$  and  $\pi(x, t) < 0$  describe a locally aggrading and eroding bed, respectively (Figure 1b). This framework describes a range of topographic changes, including bedform evolution under steady and unsteady flows and climbing bedforms (McElroy & Mohrig, 2009; Reesink et al., 2018).

Bedform migration and deformation rates also control the preservation of time and surface processes in the sedimentary record (Paola et al., 2018; Reesink et al., 2015), and a dimensionless index for cross strata preservation is given by

$$\theta(x, t) = \frac{\Pi(x, t)}{V_c(t)} \quad (4)$$

When the sedimentation rate is significantly lower than the bedform migration rate ( $\theta(x, t) \ll 1$ ), bedform deposits get repeatedly reworked, and only a small fraction of bedforms are stratigraphically preserved. In contrast, when  $\theta(x, t)$  is of order unity, bedforms have a high potential to be stratigraphically preserved.

Here, we combined these theoretical frameworks with experimental bedform evolution to explore the role of flood variability in cross strata preservation.

### 3. Methods

We analyzed existing experimental data of dune evolution under steady (Ganti et al., 2013) and unsteady flows (Martin & Jerolmack, 2013). Experiments were conducted in a 15 m long, 0.92 m wide, and 0.65 m deep tilting flume (median grain size of 0.37 mm) at the St. Anthony Falls Laboratory, University of Minnesota (supporting information Text S1; Martin & Jerolmack, 2013; Ganti et al., 2013). We analyzed two symmetrical triangular flood runs, called “slow” and “fast” flood, and used a steady flow experiment as a control (Figure 2b). In both unsteady experiments, water discharge was gradually varied from 0.04 to 0.115 m<sup>3</sup>/s and back to 0.04 m<sup>3</sup>/s. The flood hydrograph duration was 8 and 2 hr for the slow and fast floods, respectively (Figure 2b). The control experiment had a steady water discharge of 0.08 m<sup>3</sup>/s (~average of the maximum and minimum water discharges in unsteady experiments) over 20 hr. We also analyzed experimental data from another steady-state experiment with a water discharge of 0.04 m<sup>3</sup>/s for 15 hr (Ganti et al., 2013). In all experiments, bedforms were always present, and sediment was recirculated such that net aggradation rate was zero ( $r = 0$ ;  $\Pi(x, t) = \pi(x, t)$ ).

Bed topography was continuously measured using ultrasonic probes along an 8 and 6 m longitudinal transect for unsteady and control experiments, respectively. The horizontal and vertical resolution of data is 1 cm and 1 mm, respectively, and the temporal resolution of the data is 17 s for the slow and fast flood experiments (Martin & Jerolmack, 2013), and 45 s for the control experiment (Ganti et al., 2013).

To quantify bedform geometry, we detrended the bed profiles at each time step and computed  $h_d$  as the difference between consecutive bedform crest and trough elevations, and  $\lambda$  as the distance between successive bedform crests (van der Mark et al., 2008). We used detrended topographic profiles to calculate  $V_c(t)$  (equation (3)) using a well-established cross-correlation method (Text S2; McElroy & Mohrig, 2009). We estimated bedform deformation rates using a discretized version of equation (3). To avoid edge effects, we computed  $V_c(t)$  and  $\pi(x, t)$  for the middle 6 and 4 m transect of the unsteady and control experiments, respectively. We also characterized the spatiotemporal evolution of  $\theta(x, t)$  (equation (4)) for all experiments and evaluated its spatial average,  $\bar{\theta}(\bar{x}, t)$ . An overbar on  $x$  or  $t$  denotes spatial or temporal averaging, respectively.

Martin and Jerolmack (2013) reported  $T_f$  for the unsteady experiments, and we computed  $T_f$  for the steady-state experiments using equation (1). We computed  $T^*$  for each time step of the experiments. For the rising and falling limb, we equated  $T_f$  to the difference between experimental runtime and the time at which the increase and decrease in water discharge was initiated, respectively (Figures 1 and S1). For the steady-state experiment,  $T_f$  was equated to the experimental runtime.

We constructed synthetic stratigraphy from stacked bed elevation time series clipped for erosion and measured  $d_{st}$  as the thickness of deposits between successive erosional boundaries (Ganti et al., 2013). For unsteady experiments, we estimated  $s_m/h_m$  and  $CV(d_{st})$  for deposits corresponding to the flood recession and the postflood period (Figure 1a). Further, we tracked the original experimental runtime and the corresponding  $T^*$  values for the stratigraphically preserved elevations of both unsteady and steady experiments. We also evaluated the spatiotemporally averaged preservation index that corresponded to the

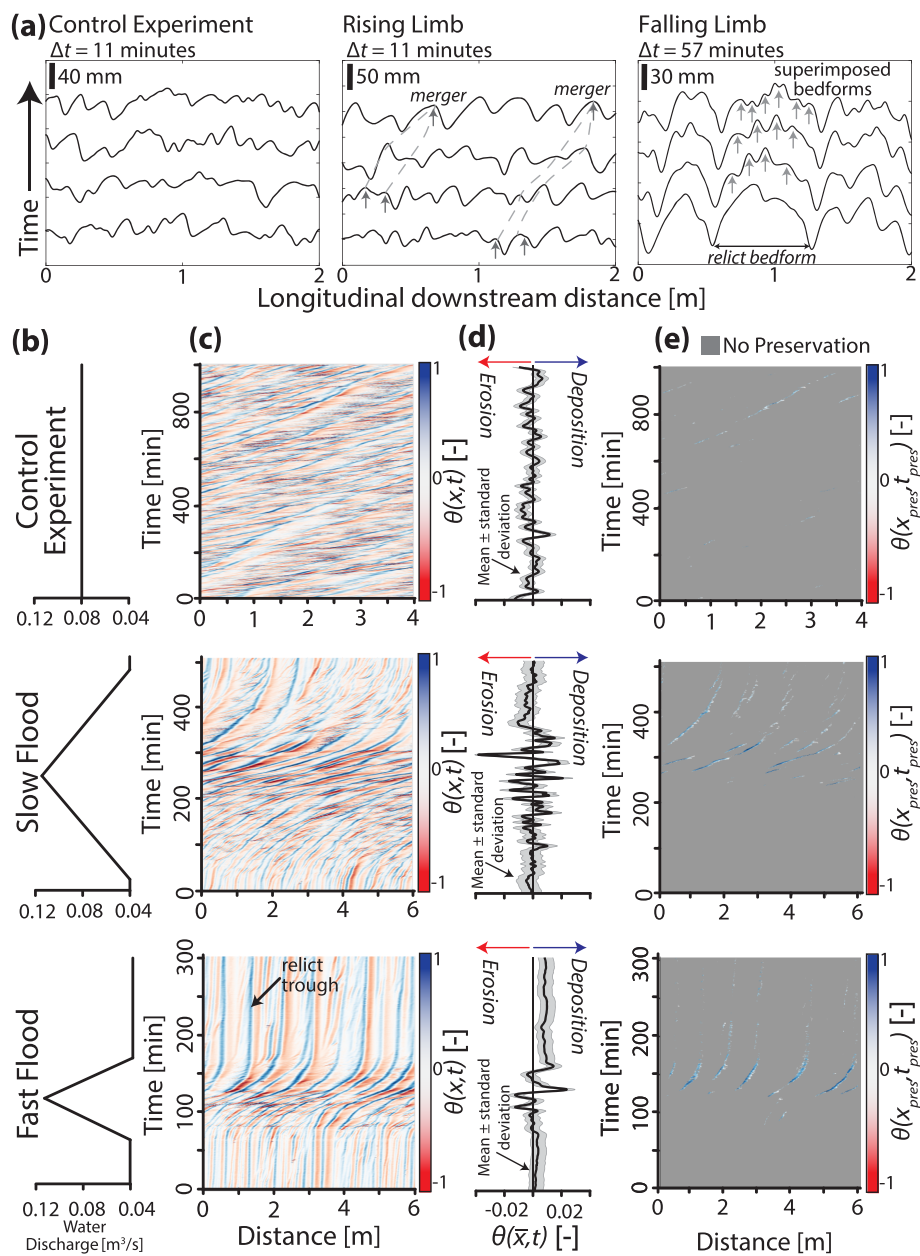


**Figure 2.** (a) Bed elevation profiles through time for the control experiment, and rising and falling limbs of the fast flood experiment. Plots showing the coevolution of (b) water discharge, (c) preservation index,  $\theta(x,t)$ , (d) spatially averaged preservation index,  $\bar{\theta}(x,t)$ , and (e) magnitudes of preservation index for stratigraphically preserved times for the control experiment (top panel), slow flood (middle panel), and fast flood (bottom panel) experiments. Panel (e) highlights that  $\theta(x_{pres}, t_{pres}) > 0$  during cross-stratal preservation.

stratigraphically preserved time ( $\theta(\bar{x}_{pres}, \bar{t}_{pres})$ ; subscript denotes “preserved”) during the steady experiment and the aforementioned stages of the unsteady experiments.

#### 4. Results

Martin and Jerolmack (2013) and Ganti et al. (2013) analyzed bedform geometry for the experiments reported here. We summarize their results followed by our analysis of the bedform kinematics and cross strata preservation.

#### 4.1. Bedform Kinematics in Steady and Unsteady Flows

Bedforms achieved statistical steady state for the control experiment, with  $h_m \approx 20$  mm and  $\lambda \approx 300$  mm (Figure 2a; Ganti et al., 2013). For the unsteady experiments,  $T_t$  was 1.2 and 5.4 hr for the bedform growth and decay process, respectively (Martin & Jerolmack, 2013). Slow flood discharge increased over 4 hr, yielding  $T^* = 3.33$  at the end of the growth process, and bedforms grew by the merger process ( $h_m(\lambda)$  increased from 20 (300) to 50 (650) mm; Figure S1a), in concert with the waxing flow rates (Martin & Jerolmack, 2013). The peak-flood-equilibrated bedforms experienced a decrease in flow over a 4 hr duration, yielding  $T^* = 0.74$  at the end of the waning flow, and bedform size reduced by the cannibalization process ( $h_m$  and  $\lambda$  decreased to 20 and 300 mm), and no substantial bedform hysteresis was observed (Figure S1a; Martin & Jerolmack, 2013). For the fast flood, the waxing and waning flow duration was 1 hr, yielding  $T^*$  of 0.83 and 0.18 at the end of the growth and decay process, respectively. Similar to the slow flood, bedform growth and decay occurred by the merger and cannibalization process, respectively (Figure 2a); however, bedform hysteresis was observed during falling limb, consistent with theory (Myrow et al., 2018), where  $h_m(\lambda)$  at the beginning and the end of the flood was 25 (400) and 40 mm (550 mm), respectively (Figure S1b; Martin & Jerolmack, 2013).

The migration and deformation rates in the control experiment were temporally invariant ( $V_c(t) \sim 0.32$  mm/s;  $|\pi(x,t)| \sim 2 \times 10^{-3}$  mm/s; Ganti et al., 2013). For unsteady experiments, the threefold increase in water discharge resulted in a twofold increase in  $V_c$  (0.55 to 1 mm/s), which reduced to the preflood value during the flood recession and stayed constant through the postflood period (Figures S2a and S3a). Bedform migration rate was diminished during fast-flood recession, when compared to the slow-flood recession, because of the stagnation of the peak-flood-equilibrated bedforms (Figures 2a, S2a, and S3a). In both unsteady experiments,  $|\pi(\bar{x}, t)|$  was elevated for the entirety of the flood duration compared to steady conditions (Figures S2 and S3). Bedforms in the fast flood were characterized by elevated, positive deformation rates through the flood recession and beyond because the prevailing, superimposed bedforms only reworked the crests of the relict peak-flood-equilibrated bedforms (Figures 2a, S2b, and S4). In contrast, bedforms in falling stage of the slow-flood experiment evolved in concert with the decreasing flow discharge such that peak-flood-equilibrated bedforms were more thoroughly reworked with elevated positive and negative deformation rates during the cannibalization process (Figures S3 and S4). Overall, flood hydrographs increased the bedform deformation rates substantially, relative to migration rates.

#### 4.2. Preservation of Time and Process in Cross Strata

For the control experiment, the average total deposit thickness was 37 mm, with  $s_m = 6.5 \pm 5.8$  mm (mean  $\pm$  standard deviation; Ganti et al., 2013). In comparison, the average deposit thickness in the slow and fast flood experiments was 60 ( $s_m = 6.1 \pm 9.8$ ) and 38 mm ( $s_m = 3.9 \pm 8.2$  mm), respectively. In the unsteady experiments, cross strata primarily recorded flood recession and had virtually no record of the waxing flows (Figure 2e). On average, 91% and 67% of the total deposit corresponded with flood recession in slow and fast flood experiments, respectively, when  $T^* < 1$  (Figure 3a). The distributions of stratigraphically preserved  $T^*$  values were positively skewed with  $T^* = 1$  corresponding to the 90<sup>th</sup> and 96<sup>th</sup> percentile for slow and fast flood experiments, respectively (Figure 3b). In contrast, we find no systematic trend in the preserved  $T^*$  of the control experiment (Figure 3b).

In the control experiment,  $s_m/h_m$  was  $0.29 \pm 0.16$  (mean  $\pm$  standard deviation), consistent with the variability-dominated preservation model (Figure 4a). In comparison, the preservation ratio was high during flood recession with  $s_m/h_m$  of  $0.39 \pm 0.14$  and  $0.48 \pm 0.05$  for slow and fast flood, respectively (Figure 4a). We found that 20% and 37% of the largest peak flood bedform heights (>90th percentile of all bedforms in each experiment) was preserved in cross strata for the slow and fast flood experiments, respectively. Beyond the flood recession,  $s_m/h_m$  was  $0.25 \pm 0.02$  and  $0.23 \pm 0.04$  for the slow and fast flood experiments, respectively, consistent with the variability-dominated preservation model (Figure 4a). Elevated bedform preservation ratios during the flood recession were associated with high preservation index values. We found that the estimated  $\theta(\bar{x}, t)$  was low (order of  $10^{-3}$ ) in the control experiment with no temporal trend (Figure 2d); however,  $\theta(\bar{x}, t)$  (order of  $10^{-2}$ ; Figure 2d) was an order of magnitude higher during flood recession in both unsteady experiments. High values of  $\theta(\bar{x}, t)$  resulted from the substantial increase in the bedform deformation rates, relative to migration rates, during the flood hydrograph (Figures 2a, 2d, S2, and S3). Results also indicate a

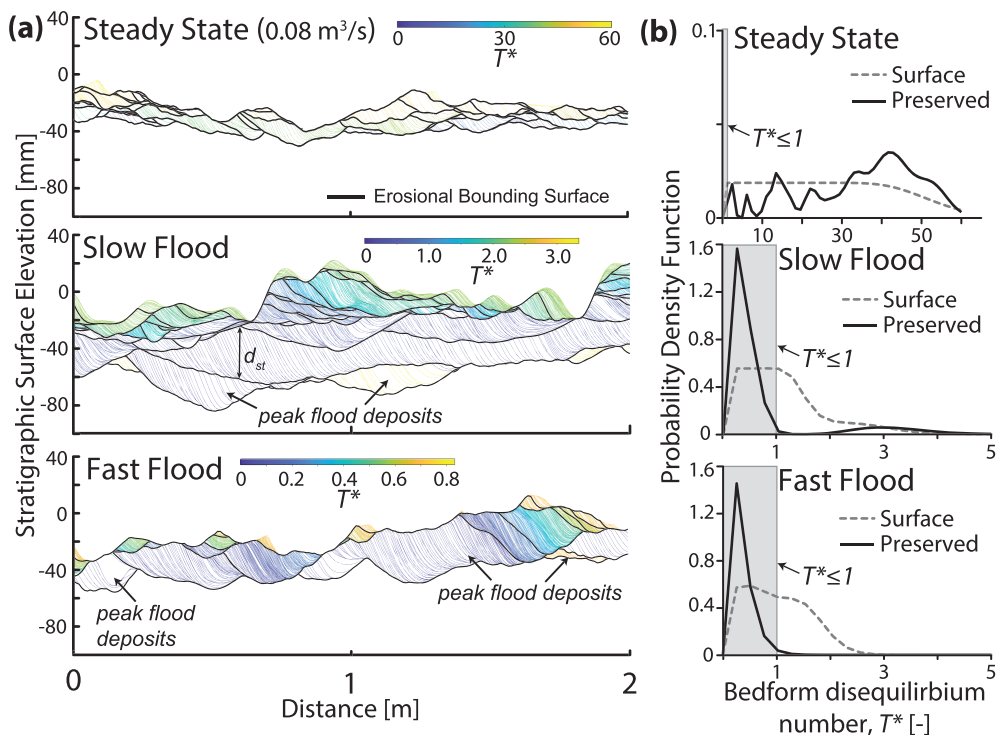


**Figure 3.** (a) Synthetic stratigraphic sections color coded by the preserved bedform disequilibrium number. (b) Comparison of the probability density functions of the bedform disequilibrium numbers during bedform evolution (gray dashed line) versus what was preserved stratigraphically (solid, black line).

strong, linear correlation between the bedform preservation ratio and  $\theta(\bar{x}_{\text{pres}}, \bar{t}_{\text{pres}})$ , computed across the durations of the flood recession and postflood period in the unsteady experiments, and the control experiment (Figure 4b).

Finally, the estimated  $CV(d_{st})$  for the steady experiments, slow-flood deposits, and the postflood deposits of the fast flood experiment were consistent with the variability-dominated preservation model (Figure 4c). In contrast, sets deposited during the fast-flood recession ( $0 \leq T^* \leq 0.18$ ) displayed significantly less variability with  $CV(d_{st})$  of 0.59 (Figure 4c).

## 5. Discussion

Our results indicate that cross strata record bedform disequilibrium dynamics that occur during flood recession, even if this duration constitutes a tiny fraction of total time (Figures 3 and 4a). Flow variability substantially increases dune deformation rates (Reesink et al., 2018), relative to migration rates (Figures 2, S2b, and S3b), which causes higher localized sedimentation that leads to the enhanced preservation of bedform kinematics (equation (4) and Figures 4a and 4b; Paola et al., 2018). Results also indicate that the bedform preservation ratio is linearly correlated with the preservation index (Figure 4b), consistent with numerical models that documented increase in  $s_m/h_m$  with bedform climb angle ( $r/V_c$ ; Jerolmack & Mohrig, 2005). While relatively constant  $s_m/h_m$  was documented for low bedform climb angles ( $r/V_c < 10^{-2}$ ; Leclair & Bridge, 2001), our results, together with field observations (Reesink et al., 2015), indicate that cross-stratal preservation is sensitive to localized spatiotemporal changes in sedimentation rates, rather than net aggradation rates (Figure 4b).

The rate of decrease in water discharge can have a profound influence on bedform adjustment and consequently bedform preservation in the rock record. Results indicate that an abrupt decrease in water discharge can lead to the stagnation of peak-flood-equilibrated bedforms, which are minimally reworked by smaller, superimposed bedforms during the postflood period (Figures 3 and 4a; Reesink & Bridge, 2007, 2009).

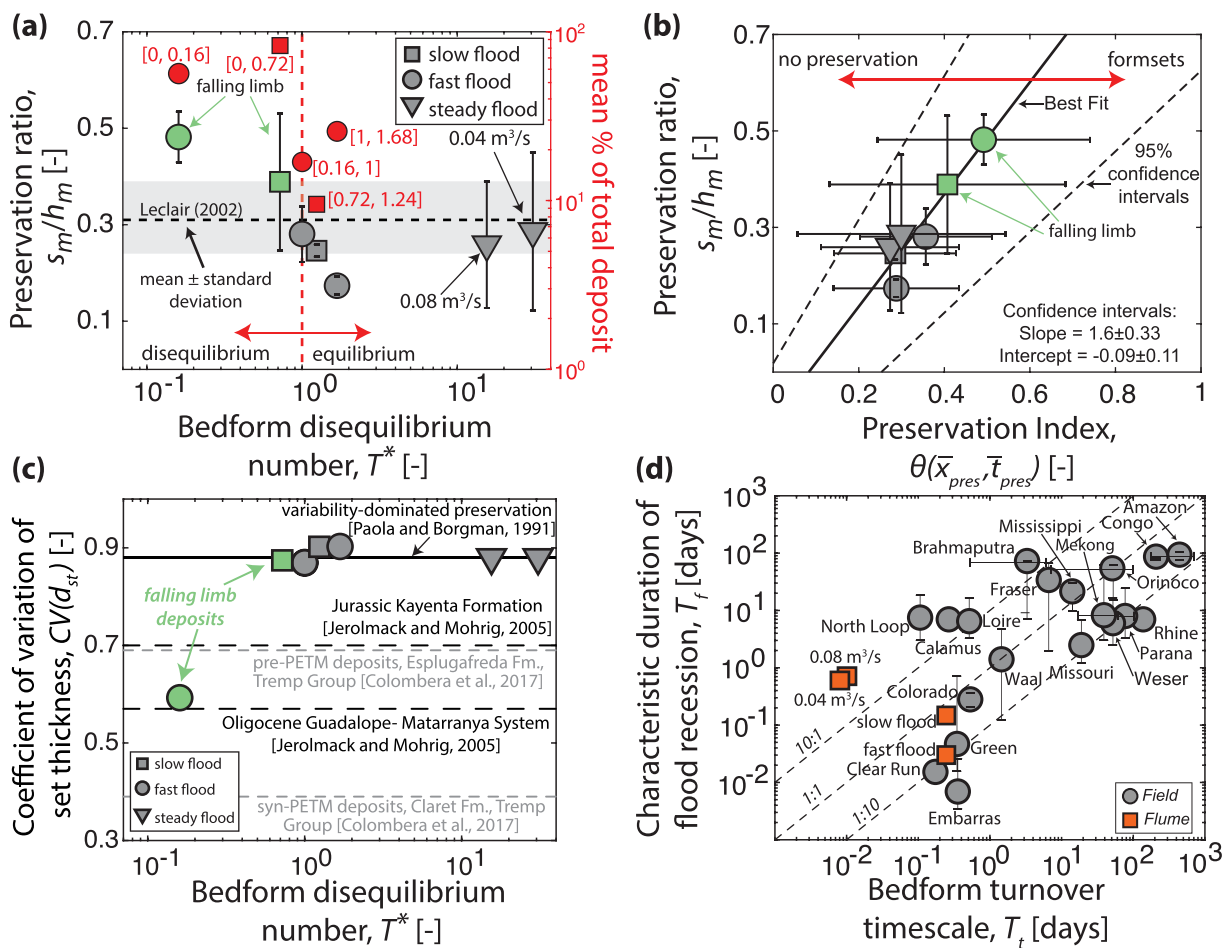


**Figure 4.** (a) Bedform preservation ratio (left axis) and average fraction of total deposit (red markers; right axis) constructed during flood recession and postflood period of unsteady experiments as a function of the bedform disequilibrium number. Bracketed numbers denote the  $T^*$  range over which computations were performed, and data are plotted with an abscissa of maximum  $T^*$  in this range. The black dashed line and gray shaded area denote  $s_m/h_m$  estimated for the steady-state experiments of Leclair (2002) with no net aggradation. (b) Functional relationship between the bedform preservation ratio and the spatiotemporally averaged, stratigraphically preserved preservation index,  $\theta(\bar{x}_{pres}, \bar{t}_{pres})$ , across experiments. (c) Coefficient of variation of set thickness as a function of bedform disequilibrium number. (d) A representative global compilation of characteristic flood recession duration and bedform turnover time scale for 19 rivers (circles) and the four experimental runs (squares) (Table S1 and Text S3). Computations in (b) and (c) were performed over the same time scales denoted in (a). The span of the error bars on  $s_m/h_m$ ,  $T_t$ , and  $\theta(\bar{x}_{pres}, \bar{t}_{pres})$  denotes two standard deviations, whereas the span of the  $T_f$  error bars denotes the interquartile range.

This process leads to large preserved cross sets and enhanced preservation of peak-flood-equilibrated bedforms (Reesink & Bridge, 2007), consistent with our observations in the fast flood stratigraphy (Figure 3a). Similar dynamics may also lead to enhanced bar preservation in abruptly waning flows (Jones, 1977). In contrast, gradual decline in flood discharge leads to in-phase evolution of bedforms and water discharge such that peak-flood-equilibrated bedforms are substantially reworked during waning flow and postflood period leaving no clear stratigraphic signature of peak-flood conditions (Leclair, 2011).

Results indicate that the contrasting kinematics of bedform evolution under broad and flashy flood hydrographs can lead to discernible differences in cross set thickness. Fluvial cross strata constructed during flashy flood hydrographs are characterized by a few large cross sets from peak-flood conditions that underlie the majority of the sets constructed by smaller, superimposed bedforms during the postflood period (Figure 3a), which leads to low  $s_m$  values across the entire deposit (section 4.2). In comparison, sets constructed during the steady flow and broad flood hydrographs are repeatedly reworked by the passage of bedforms with variable scour depths. A similar reduction in overall  $s_m$  values with increasing flood variability was documented in numerical models of bar evolution in anastomosing rivers (Nicholas et al., 2016).

Our results have implications for quantifying formative-flood variability from cross strata. Mahon and McElroy (2018) demonstrated how bedload flux could be estimated from cross strata, which may enable the quantification of  $T_t$  (equation (1)). Because preserved cross strata dominantly correspond to flood recession (Figure 3), we suggest that the formative-flood time scale, normalized by  $T_t$ , can be deduced from detailed field measurements of set thickness variability. Results indicate that broad flood hydrographs with long waning-flow duration and  $T^* \geq 1$ , will result in  $CV(d_{st}) \approx 0.88$  (Figure 4c). In contrast, flashy flood hydrographs, with abrupt flow deceleration and  $T^* \ll 1$ , will result in  $CV(d_{st})$  that is substantially lower than 0.88 (Figure 4c). Jerolmack and Mohrig (2005) reported  $CV(d_{st})$  of 0.70 and 0.57 for preserved dune sets in channel fill deposits of the Jurassic Kayenta Formation, Utah, and the Oligocene Guadalupe-Matarranya System, Spain, respectively, and attributed the low  $CV(d_{st})$  in latter deposits to increased bedform climb angle. Our results suggest that such an increase in bedform climb angle would likely be spatiotemporally concentrated (Paola et al., 2018) and may reflect the record of bedform evolution under flashy hydrographs (Figure 4c). Similarly, Colombera et al. (2017) measured  $d_{st}$  across the Paleocene-Eocene Tremp Group, Spain, to study fluvial response to Paleocene-Eocene Thermal Maximum (PETM), a global warming event in the Cenozoic era (McInerney & Wing, 2011). They found no trend in the flow depths across the pre-PETM and syn-PETM deposits; however,  $s_m$  increased, and  $CV(d_{st})$  decreased across the same interval (Figure 4c). Our results point to a flashier formative hydrograph during PETM ( $T^* \ll 1$ ), when compared to pre-PETM, which should result in higher  $s_m/h_m$  and lower  $CV(d_{st})$  for the same formative bankfull flow depths across the entire time period.

Lastly, we evaluated the prevalence of bedform disequilibrium in modern rivers by estimating representative  $T^*$  values for 19 rivers worldwide (Text S3 and Table S1). In our compilation,  $T^* < 1$  for 12 rivers and bedform hysteresis was independently documented in the majority of these rivers (e.g., Allen, 1982b; Harvey et al., 2012; Wilbers & Ten Brinke, 2003). Our compilation indicates that flood variability may outpace bedform evolution in large, low-gradient rivers (e.g., Amazon, Paraná, Rhine; Figure 4d) and result in high bedform preservation ratio (Figure 4a), consistent with abundance of form set preservation in the Paraná River deposits (Reesink et al., 2015). Large monsoonal rivers (e.g., Brahmaputra) with sustained annual floods, however, may have sufficiently broad hydrographs such that  $T^* > 1$  (Figure 4d), indicating that flood seasonality is an essential control on alluvial stratigraphy (e.g., Plink-Björklund, 2015). In contrast to large rivers, dunes in smaller, steeper rivers have  $T_t$  values on the order of a few hours (e.g., Colorado, Calamus; Figure 4d), indicating that their evolution is seldom out of phase with prevailing flows. Based on these observations, we suggest that the variability-dominated preservation model is directly applicable to preserved cross strata of smaller, steeper rivers; however, it should be used in conjunction with an independent evaluation of  $CV(d_{st})$  when applied to large-river deposits through Earth history.

## 6. Conclusions

Our work provides a theoretical framework for mapping transient surface processes into measurable quantities of fluvial strata. Using theory, experiments, and field observations, we demonstrate that bedform disequilibrium dynamics are the norm in modern rivers and ancient fluvial strata. Specifically, we find that

1. Fluvial cross strata preferentially archive bedform evolution during flood recession, even when its duration is a tiny fraction of total time.
2. Flow variability increases bedform deformation rates, relative to migration rates, and results in the preferential preservation of bedform disequilibrium dynamics.
3. Coefficient of variation of preserved sets can constrain the time scale of formative flood variability relative to the bedform turnover time scale.

These results contribute to the growing recognition that flood variability is a key control on alluvial stratigraphy from bedform to basin scales (Colombera & Mountney, 2019; Fielding et al., 2018; Ganti, Lamb, et al., 2019; Nicholas et al., 2016; Trower et al., 2018).

## References

- Allen, J. R. L. (1973a). Features of cross-stratified units due to random and other changes in bed forms. *Sedimentology*, 20, 189–202.  
Allen, J. R. L. (1973b). Phase differences between bed configuration and flow in natural environments, and their geological relevance. *Sedimentology*, 20(2), 323–329.

## Acknowledgments

We thank Rob Duller and Luca Colombera for constructive reviews. This work was supported by the donors of the American Chemical Society Petroleum Research Fund to Ganti. Data sets for this research are available at the Sediment Experimentalist Network's data repository (<http://sedexp.net/catalog/bedform-adjustment-experiments>).

- Allen, J. R. L. (1974). Reaction, relaxation and lag in natural sedimentary systems: General principles, examples and lessons. *Earth-Science Reviews*, 10(4), 263–342.
- Allen, J. R. L. (1976). Time-lag of dunes in unsteady flows: An analysis of Nasner's data from the R. Weser, Germany. *Sedimentary Geology*, 15(4), 309–321.
- Allen, J. R. L. (1982a). *Sedimentary structures: Their character and physical basis, Volume I* (Vol. 30, p. 593). Amsterdam: Elsevier, Developments in Sedimentology.
- Allen, J. R. L. (1982b). Ripples and dunes in changing flows. *Sedimentary Structures, Their Character and Physical Basis I*, 307–344.
- Baas, J. H., Best, J. L., & Peakall, J. (2016). Predicting bedforms and primary current stratification in cohesive mixtures of mud and sand. *Journal of the Geological Society*, 173(1), 12–45. <https://doi.org/10.1144/jgs2015-024>
- Best, J. (2005). The fluid dynamics of river dunes: A review and some future research directions. *Journal of Geophysical Research*, 110, F04S02. <https://doi.org/10.1029/2004JF000218>
- Best, J., & Fielding, C. R. (2019). Describing fluvial systems: Linking processes to deposits and stratigraphy. *Geological Society, London, Special Publications*, 488. <https://doi.org/10.1144/SP488-2019-056>
- Bhattacharya, J. P., & Tye, R. S. (2004). AAPG studies in geology No. 50 (section title: The Ferron sandstone—Overview and reservoir analog) Chapter 2: Searching for modern Ferron analogs and application to subsurface interpretation, 39–58.
- Bradley, R. W., & Venditti, J. G. (2017). Reevaluating dune scaling relations. *Earth-Science Reviews*, 165, 356–376. <https://doi.org/10.1016/j.earscirev.2016.11.004>
- Bradley, R. W., & Venditti, J. G. (2019a). The growth of dunes in rivers. *Journal of Geophysical Research: Earth Surface*, 124, 548–566. <https://doi.org/10.1029/2018JF004835>
- Bradley, R. W., & Venditti, J. G. (2019b). Transport scaling of dune dimensions in shallow flows. *Journal of Geophysical Research: Earth Surface*, 124, 526–547. <https://doi.org/10.1029/2018JF004832>
- Bridge, J., & Best, J. (1997). Preservation of planar laminae due to migration of low-relief bed waves over aggrading upper-stage plane beds: Comparison of experimental data with theory. *Sedimentology*, 44(2), 253–262. <https://doi.org/10.1111/j.1365-3091.1997.tb01523.x>
- Carling, P. A. (1999). Subaqueous gravel dunes. *Journal of Sedimentary Research*, 69(3).
- Colombera, L., Arévalo, O. J., & Mountney, N. P. (2017). Fluvial-system response to climate change: The Paleocene-Eocene Tremp Group, Pyrenees, Spain. *Global and Planetary Change*, 157, 1–17. <https://doi.org/10.1016/j.gloplacha.2017.08.011>
- Colombera, L., & Mountney, N. P. (2019). The lithofacies organization of fluvial channel deposits: A meta-analysis of modern rivers. *Sedimentary Geology*, 383, 16–40. <https://doi.org/10.1016/j.sedgeo.2019.01.011>
- Edgar, L. A., Gupta, S., Rubin, D. M., Lewis, K. W., Kocurek, G. A., Anderson, R. B., et al. (2018). Shaler: In situ analysis of a fluvial sedimentary deposit on Mars. *Sedimentology*, 65(1), 96–122. <https://doi.org/10.1111/sed.12370>
- Fielding, C. R., Alexander, J., & Allen, J. P. (2018). The role of discharge variability in the formation and preservation of alluvial sediment bodies. *Sedimentary Geology*, 365, 1–20. <https://doi.org/10.1016/j.sedgeo.2017.12.022>
- Frings, R. M., & Kleinhans, M. G. (2008). Complex variations in sediment transport at three large river bifurcations during discharge waves in the river Rhine. *Sedimentology*, 55(5), 1145–1171. <https://doi.org/10.1111/j.1365-3091.2007.00940.x>
- Ganti, V., Lamb, M. P., & Chadwick, A. J. (2019). Autogenic erosional surfaces in fluvio-deltaic stratigraphy from floods, avulsions, and backwater hydrodynamics. *Journal of Sedimentary Research*, 89(8), 815–832.
- Ganti, V., Lamb, M. P., & McElroy, B. (2014). Quantitative bounds on morphodynamics and implications for reading the sedimentary record. *Nature Communications*, 5, 3298.
- Ganti, V., Paola, C., & Foufoula-Georgiou, E. (2013). Kinematic controls on the geometry of the preserved cross sets. *Journal of Geophysical Research: Earth Surface*, 118, 1296–1307. <https://doi.org/10.1002/jgrf.20094>
- Ganti, V., Whittaker, A. C., Lamb, M. P., & Fischer, W. W. (2019). Low-gradient, single-threaded rivers prior to greening of the continents. *Proceedings of the National Academy of Sciences*, 116(24), 11,652–11,657. <https://doi.org/10.1073/pnas.1901642116>
- Gilbert, G. K. (1899). Ripple-marks and cross-bedding. *Bulletin of the Geological Society of America*, 10(1), 135–140.
- Hajek, E. A., & Straub, K. M. (2017). Autogenic sedimentation in clastic stratigraphy. *Annual Review of Earth and Planetary Sciences*, 45(1), 681–709. <https://doi.org/10.1146/annurev-earth-063016-015935>
- Harvey, J. W., Drummond, J. D., Martin, R. L., McPhillips, L. E., Packman, A. I., Jerolmack, D. J., et al. (2012). Hydrogeomorphology of the hyporheic zone: Stream solute and fine particle interactions with a dynamic streambed. *Journal of Geophysical Research*, 117, G00N11. <https://doi.org/10.1029/2012JG002043>
- Jerolmack, D. J., & Mohrig, D. (2005). Frozen dynamics of migrating bedforms. *Geology*, 33(1), 57–60. <https://doi.org/10.1130/G20897.1>
- Jones, C. M. (1977). Effects of varying discharge regimes on bed-form sedimentary structures in modern rivers. *Geology*, 5(9), 567–570.
- Julien, P., Klaassen, G., Ten Brinke, W., & Wilbers, A. (2002). Case study: Bed resistance of Rhine River during 1998 flood. *Journal of Hydraulic Engineering*, 128(12), 1042–1050.
- Leclair, S. F. (2002). Preservation of cross-strata due to the migration of subaqueous dunes: An experimental investigation. *Sedimentology*, 49(6), 1157–1180. <https://doi.org/10.1046/j.1365-3091.2002.00482.x>
- Leclair, S. F. (2011). Interpreting fluvial hydromorphology from the rock record: Large-river peak flows leave now clear signature. *SEPM Special Publication*, 97.
- Leclair, S. F., & Bridge, J. S. (2001). Quantitative interpretation of sedimentary structures formed by river dunes. *Journal of Sedimentary Research*, 71(5), 713–716.
- Mahon, R. C., & McElroy, B. (2018). Indirect estimation of bedload flux from modern sand-bed rivers and ancient fluvial strata. *Geology*, 46(7), 579–582. <https://doi.org/10.1130/G40161.1>
- Martin, R. L., & Jerolmack, D. J. (2013). Origin of hysteresis in bed form response to unsteady flows. *Water Resources Research*, 49, 1314–1333. <https://doi.org/10.1002/wrcr.20093>
- McElroy, B., & Mohrig, D. (2009). Nature of deformation of sandy bed forms. *Journal of Geophysical Research*, 114, F00A04. <https://doi.org/10.1029/2008JF001220>
- McInerney, F. A., & Wing, S. L. (2011). The Paleocene-Eocene thermal maximum: A perturbation of carbon cycle, climate, and biosphere with implications for the future. *Annual Review of Earth and Planetary Sciences*, 39(1), 489–516. <https://doi.org/10.1146/annurev-earth-040610-133431>
- Myrow, P. M., Jerolmack, D. J., & Perron, J. T. (2018). Bedform disequilibrium. *Journal of Sedimentary Research*, 88(9), 1096–1113.
- Nicholas, A. P., Sambrook Smith, G. H., Amsler, M. L., Ashworth, P. J., Best, J. L., Hardy, R. J., et al. (2016). The role of discharge variability in determining alluvial stratigraphy. *Geology*, 44(1), 3–6. <https://doi.org/10.1130/G37215.1>

- Ohata, K., Naruse, H., Yokokawa, M., & Viparelli, E. (2017). New bedform phase diagrams and discriminant functions for formative conditions of bedforms in open-channel flows. *Journal of Geophysical Research: Earth Surface*, 122, 2139–2158. <https://doi.org/10.1002/2017JF004290>
- Paola, C., & Borgman, L. (1991). Reconstructing random topography from preserved stratification. *Sedimentology*, 38(4), 553–565. <https://doi.org/10.1111/j.1365-3091.1991.tb01008.x>
- Paola, C., Ganti, V., Mohrig, D., Runkel, A. C., & Straub, K. M. (2018). Time not our time: Physical controls on the preservation and measurement of geologic time. *Annual Review of Earth and Planetary Sciences*, 46(1), 409–438. <https://doi.org/10.1146/annurev-earth-082517-010129>
- Parsons, D. R., Schindler, R. J., Hope, J. A., Malarkey, J., Baas, J. H., Peakall, J., et al. (2016). The role of biophysical cohesion on subaqueous bed form size. *Geophysical Research Letters*, 43(4), 1566–1573. <https://doi.org/10.1002/2016GL067667>
- Plink-Björklund, P. (2015). Morphodynamics of rivers strongly affected by monsoon precipitation: Review of depositional style and forcing factors. *Sedimentary Geology*, 323, 110–147. <https://doi.org/10.1016/j.sedgeo.2015.04.004>
- Reesink, A., & Bridge, J. S. (2007). Influence of superimposed bedforms and flow unsteadiness on formation of cross strata in dunes and unit bars. *Sedimentary Geology*, 202(1), 281–296. <https://doi.org/10.1016/j.sedgeo.2007.02.005>
- Reesink, A., & Bridge, J. S. (2009). Influence of bedform superimposition and flow unsteadiness on the formation of cross strata in dunes and unit bars—Part 2, Further experiments. *Sedimentary Geology*, 222(3), 274–300. <https://doi.org/10.1016/j.sedgeo.2009.09.014>
- Reesink, A. J. H., Parsons, D. R., Ashworth, P. J., Best, J. L., Hardy, R. J., Murphy, B. J., et al. (2018). The adaptation of dunes to changes in river flow. *Earth-Science Reviews*, 185, 1065–1087. <https://doi.org/10.1016/j.earscirev.2018.09.002>
- Reesink, A. J. H., van den Berg, J. H., Parsons, D. R., Amsler, M. L., Best, J. L., Hardy, R. J., et al. (2015). Extremes in dune preservation: Controls on the completeness of fluvial deposits. *Earth-Science Reviews*, 150, 652–665. <https://doi.org/10.1016/j.earscirev.2015.09.008>
- Rubin, D. M., & Hunter, R. E. (1982). Bedform climbing in theory and nature. *Sedimentology*, 29(1), 121–138. <https://doi.org/10.1111/j.1365-3091.1982.tb01714.x>
- Sorby, H. C. (1859). On the structures produced by the currents present during the deposition of stratified rocks. *Geologist*, 2, 137–147.
- Southard, J. B. (1991). Experimental determination of bed-form stability. *Annual Review of Earth and Planetary Sciences*, 19(1), 423–455.
- Ten Brinke, W., Wilbers, A., & Wesseling, C. (1999). Dune growth, decay, and migration rates during a large-magnitude flood at a sand and mixed sand-gravel bed in the Dutch Rhine River System. *Fluvial Sedimentology*, 6, 15–32.
- Trower, E. J., Ganti, V., Fischer, W. W., & Lamb, M. P. (2018). Erosional surfaces in the Upper Cretaceous Castlegate Sandstone (Utah, USA): Sequence boundaries or autogenic scour from backwater hydrodynamics? *Geology*, 46(8), 707–710. <https://doi.org/10.1130/G40273.1>
- van der Mark, C., Blom, A., & Hulscher, S. J. (2008). Quantification of variability in bedform geometry. *Journal of Geophysical Research*, 113, F03020. <https://doi.org/10.1029/2007JF000940>
- van Rijn, L. C. (1984). Sediment transport, Part I: Bedload transport. *Journal of Hydraulic Engineering*, 110(10), 1431–1456.
- Wilbers, A. W. E., & Ten Brinke, W. B. M. (2003). The response of subaqueous dunes to floods in sand and gravel bed reaches of the Dutch Rhine. *Sedimentology*, 50, 1013–1034.
- Yalin, M. S. (1964). Geometrical properties of sand wave. *Journal of the Hydraulics Division*, 90(5), 105–119.